Recent Advances in Rapid Multi-Objective Optimization of Expensive Simulation Models in Microwave and Antenna Engineering By Pareto Front Exploration

Slawomir Koziel[1,2] and Adrian Bekasiewicz[1,2]

[1] Engineering Optimization & Modeling Center, School of Science and Engineering, Reykjavík University, Menntavegur 1, 101 Reykjavík, Iceland
(koziel@ru.is, bekasiewicz@ru.is)

[2] Faculty of Electronics, Telecommunications and Informatics
Gdansk University of Technology, 80-233 Gdansk, Poland

Keywords: Computer-aided design (CAD), computational electromagnetics, electromagnetic (EM)-simulation models, simulation-driven design, multi-objective optimization, surrogate modeling, space mapping, response features.

Abstract

Practical engineering design problems are inherently multi-objective, i.e., require simultaneous control of several (and often conflicting) criteria. In many situations, genuine multi-objective optimization is required to acquire comprehensive information about the system of interest. The most popular solution techniques are population-based metaheuristics, however, they are not practical for handling expensive electromagnetic (EM)-simulation models in microwave and antenna engineering. A workaround is to use auxiliary response surface approximation surrogates but it is challenging for higher-dimensional problems. Recently, a deterministic approach has been proposed for expedited multi-objective design optimization of expensive models in computational electromagnetics. The method relies on variable-fidelity EM simulations, tracking the Pareto front geometry, as well as response correction. The algorithm sequentially generates Pareto-optimal designs using a series of constrained single-objective optimizations. The previously obtained design is used as a starting point for the next iteration. In this work, we review this technique and its modification based on space mapping surrogates. We also propose new variations exploiting adjoint sensitivities, as well as response features which can be attractive depending on availability of derivatives or the characteristics of the system responses that need to be handled. We also discuss several case studies involving various antenna and microwave components.

1. Introduction

Full-wave electromagnetic (EM) analysis has become a fundamental tool of modern microwave and antenna engineering [1], [2] as well as photonics [3]. Furthermore, it is ubiquitous in the design of wireless power transfer systems [4], microwave imaging [5], non-destructive testing [6], and many other areas. Despite their accuracy, high-fidelity EM simulation models are numerically expensive which is problematic for complex structures (e.g., antenna arrays in a radome [7]). In many cases, computational models need to account for environmental components that affect performance of the device at hand [8], [9]. It is common that theoretical models unavailable or of unacceptable accuracy so that full-wave EM analysis is the only tool for reliable estimation of the system performance.

The most important challenge of simulation-driven design is high cost of accurate EM analysis (from minutes to even days, depends on complexity of the structure). This is particularly challenging from the point of view of automated numerical optimization, because conventional algorithms require a large number of EM model evaluations to yield an optimized design. This applies to both local methods and to population-based metaheuristics [10]-[14]. A practical alternative is design by means of parameter sweeping which, although simple and intuitive, requires massive interaction with the designer [15], [16]. Unfortunately, the method is unsuitable for complex problems (e.g., constrained optimization or multi-dimensional parameter spaces) and normally leads to sub-optimal designs. Therefore, design automation is highly desirable.

Numerically feasible EM-simulation-driven design methods are of high interest for the research community. In the context of gradient-based algorithms, dramatic speedup of the optimization process can be achieved using adjoint sensitivity [17], [18], [19] which allows for obtaining both the system response and its gradient [19]-[22]. While adjoint technology is one of the basic tools in, e.g., mechanical engineering [23], it is commercially available in only a few EM solvers [24], [25]. Another class of methods for numerically efficient EM-driven design is surrogate-based optimization (SBO) [26]-[29]. Surrogate-assisted techniques replace direct handling of the expensive model by a

process in which a so-called surrogate is iteratively constructed and utilized as a prediction tool guiding the algorithm towards a better design.

We can identify two classes of surrogate models: data-driven (or approximation) and physics-based ones. Approximation surrogates are primarily utilized in a global optimization context (e.g., efficient global optimizers, EGO [30], [31], optimization using artificial neural networks [32], as well as surrogate-assisted evolutionary algorithms [33], [34]). Physics-based models are obtained by means of appropriate correction of the underlying low-fidelity (or coarse) models. They can be obtained, among others, as equivalent circuits [35], or coarsely-discretized EM models [8]. Physics-based surrogates offer better generalization compared to data-driven ones due to system-specific knowledge embedded in the low-fidelity model. However, they are more expensive and thus better suited for local optimization [8]. Physics-based SBO methods include space mapping (SM) [36], [37], response correction [38]-[40], feature-based optimization [41], adaptively adjusted design specifications [42], and, recently, adaptive response scaling [43].

Similarly as in other areas, practical design problems in microwave and antenna engineering require handling multiple and often conflicting objectives. For example, a typical issue pertinent to wireless communication systems ([44], [45]) is finding acceptable compromise between the physical size of the component and its performance [8], [15], [19]. Such design tasks are often converted into single-objective problems, e.g., by selecting the primary objective and handling the others through constraints or penalty functions, or by using a weighted sum approach [13]. Nevertheless, having comprehensive information about the best possible trade-offs between conflicting design criteria is important in certain situations. This can only be achieved by means of genuine multi-objective optimization, typically in a form of the Pareto set representing alternative solutions with respect to given design criteria. The most popular techniques for solving such problems—due to simplicity, global search capability, and ability of yielding the Pareto set in a single run—are population-based metaheuristics [12], [13], [46]-[49]. Unfortunately, such methods are unsuitable for direct handling of expensive EM simulation models because of their tremendous computational cost (thousands of model evaluations and more).

Several techniques for reduced-cost multi-objective optimization exploiting both physics-based and data-driven surrogates have been proposed recently [32], [50]. In [32], an artificial neural network (ANN)-based surrogate capable of handling the physical topology of dynamic optical networks has been proposed. The ANN model is utilized to accelerate multi-objective design of the optical networks. An approach for expedited multi-objective design of antennas using variable-fidelity EM simulations and auxiliary data-driven model has been introduced in [50]. The method exploits kriging interpolation model identified using training data obtained from coarsely-discretized EM simulations. The initial approximation of the Pareto front has been obtained using evolutionary algorithm and then refined to the high-fidelity model level using space mapping. However, practical usefulness of the approach of [50] is limited to low-dimensional problems. The method of [50] was further extended for multi-dimensional parameter spaces by utilizing design space reduction techniques. In [51], the method for restricting search space based on dimensions of so-called extreme designs (i.e., the ones obtained through optimization of the system at hand with respect to one objective at a time) has been utilized to exploit the technique of [50] for optimization of a 13-parameter antenna. In [52], the approach of [51] has been extended by allocating the surrogate model domain along the diagonal spanned by the extreme points and reducing all orthogonal dimensions (w.r.t. the diagonal) accordingly. It should be emphasized, however, that the techniques mentioned in this paragraph still utilize population-based metaheuristics at certain stage of the optimization process.

A fully deterministic technique for multi-objective design optimization of computational electromagnetic models has been proposed in [53]. In contrary to the methods considered above, the approach of [53] does not require any confinement of the search space. The method is based on the concept of Pareto front exploration where subsequent Pareto-optimal designs are found using constrained local search starting from the previously found solution. Numerical efficiency of the optimization process is ensured using local response surface models constructed from coarsely-discretized EM simulations. The obtained designs are refined by means of using space mapping.

In this paper, we review the concept of [53] and discuss its several extensions in terms of how the Pareto front can be explored faster, depending on what kind of

simulation tools are available and what the characteristics of the system response at hand are. In particular, we consider local search using so-called response features where the optimization problem is reformulated in terms of suitably defined characteristic points [54], as well as gradient search with adjoint sensitivities [20]. Our considerations are illustrated using several real-world problems in microwave and antenna engineering. Benchmarking as well as comparative analysis of the presented techniques is also provided.

The rest of the paper is organized as follows. Section 2 describes several variants of multi-objective design optimization by means of Pareto front exploration, using local approximation surrogates, space mapping, adjoint sensitivities, and response features. Section 3 provides numerical validation of the considered algorithms using two ultrawideband (UWB) monopole antennas, a miniaturized rat-race coupler and a compact UWB impedance transformer implemented in microstrip technology. Section 4 discusses the results and concludes the work.

2. Multi-Objective Design Optimization by Pareto Front Exploration

In this section, we formulate multi-objective optimization problem (Section 2.1) and discuss a deterministic procedure for Pareto set identification (Section 2.2). Various options for finding subsequent Pareto-optimal designs are highlighted in Sections 2.3 through 2.6. Illustration examples are presented in Section 3.

2.1. Multi-Objective Design Problem Formulation

We will denote by $\boldsymbol{R}_f(\boldsymbol{x})$ a response of a high-fidelity computational model of the structure under design and by vector $\boldsymbol{x}$ a set of adjustable parameters (typically, geometrical dimensions and/or material parameters). Here, the model is normally evaluated using full-wave electromagnetic (EM) simulations. Moreover, $F_k(\boldsymbol{R}_f(\boldsymbol{x}))$, $k = 1$, …, N_{obj}, will be a kth design objective (e.g., reduction of the area, improvement of performance characteristics of the structure, etc.).

If the number of objectives is larger than one, i.e., $N_{obj} > 1$, then any two designs $\boldsymbol{x}^{(1)}$ and $\boldsymbol{x}^{(2)}$ for which $F_k(\boldsymbol{R}_f(\boldsymbol{x}^{(1)})) < F_k(\boldsymbol{R}_f(\boldsymbol{x}^{(2)}))$ and $F_l(\boldsymbol{R}_f(\boldsymbol{x}^{(2)})) < F_l(\boldsymbol{R}_f(\boldsymbol{x}^{(1)}))$ for at least one pair $k \neq l$, are not commensurable (i.e., none is better than the other in multi-objective

sense). In order to assess the designs, we use a Pareto dominance relation $\prec$ [12] defined as follows: for the two designs x and y, we have $x \prec y$ (x dominates y) if $F_k(\boldsymbol{R}_f(\boldsymbol{x})) \leq F_k(\boldsymbol{R}_f(\boldsymbol{y}))$ for all $k = 1, \ldots, N_{obj}$ and $F_k(\boldsymbol{R}_f(\boldsymbol{x})) < F_k(\boldsymbol{R}_f(\boldsymbol{y}))$ for at least one k.

Our goal is to obtain the Pareto-optimal set (a representation of the Pareto front) X_P in the search space X, such that for any $\boldsymbol{x} \in X_P$, there is no $\boldsymbol{y} \in X$ for which $\boldsymbol{y} \prec \boldsymbol{x}$ [12]. Such a representation is considered to be the final outcome of the optimization process. Given available trade-offs as well as performance requirements, the designer can select a specific design for further processing, e.g., prototyping.

2.2. Optimization Algorithm

The multi-objective optimization algorithm considered here is formulated for two design objectives. It is the most practical case for typical problems in microwave and antenna engineering (e.g., structure size versus its electrical performance). It is possible to generalize it for a larger number of criteria, although this version is not discussed in this paper. The algorithm generates a sequence of designs $\boldsymbol{x}^{(k)}$, $k = 1, 2, \ldots$, where $\boldsymbol{x}^{(1)}$ is a solution to the single-objective optimization problem of the form [53]

$$\boldsymbol{x}^{(1)} = \arg \min_{\boldsymbol{x}} F_1\left(\boldsymbol{R}_f(\boldsymbol{x})\right) \tag{1}$$

which is the optimum design with respect to objective F_1. For the sake of computational efficiency, the solution to (1) is obtained by means of surrogate-assisted optimization of a suitably corrected (e.g., space mapping [26], [36]) low-fidelity model $\boldsymbol{R}_c$ (e.g., coarse-discretization version of the high-fidelity model $\boldsymbol{R}_f$). By $F_2^{(1)} = F_2(\boldsymbol{R}_f(\boldsymbol{x}^{(1)}))$ we will denote the corresponding value of the second objective.

The optimization algorithm generates subsequent Pareto-optimal designs using a series of constrained single-objective optimizations. In each iteration, the design obtained in the previous one is used as a starting point. More specifically, the kth element of the Pareto set $\boldsymbol{x}^{(k)}$ is obtained as

$$\boldsymbol{x}^{(k)} = \arg \min_{\boldsymbol{x}, \, F_2(\boldsymbol{R}_f(\boldsymbol{x})) \leq F_2^{(k)}} F_1\left(\boldsymbol{R}_f(\boldsymbol{x})\right) \tag{2}$$

where $F_2^{(k)}$ is a user-defined threshold value for the second objective. The process is terminated if $F_1(\boldsymbol{R}_f(\boldsymbol{x}^{(k)}))$ is no longer satisfactory from the point of view of given design

specifications. This way, only a feasible part of the Pareto front (from the specification standpoint) is covered. There are various ways of establishing the sequence of thresholds $F_2^{(k)}$ [55],e.g., as $F_2^{(k)} = \alpha \cdot F_2^{(k-1)}$ with $\alpha < 1$, or $F_2^{(k)} = F_2^{(k-1)} - $ with $\beta > 0$. Figure 1 shows a conceptual illustration of the algorithm.

It should be noted that the algorithm (1)-(2) is deterministic and it does not rely on any form of population-based metaheuristic. Therefore, it may be computationally efficient, particularly if surrogate-based methods are used for solving (2). This can be realized using local methods because of the fact that subsequent Pareto-optimal designs are typically close to each other. Subsections 2.3 through 2.6 discuss various ways of solving (2) and discuss their properties.

2.3. Pareto Front Exploration by Local Approximation Surrogates

In practice (especially if one is interested in obtaining relatively dense representation of the Pareto front), the design $x^{(k)}$ is sufficiently close to the preceding one, i.e., $x^{(k-1)}$ so that the solution to the problem (2) can be obtained by means of sequential approximate optimization as follows. Let $x^{(k,j)}$, $j = 0, 1, \ldots$, be a sequence approximating $x^{(k)}$ (here, $x^{(k.0)} = x^{(k-1)}$) obtained as

$$x^{(k.j+1)} = \arg \min_{\substack{x, F_2(R_s^{(k.j)}(x)) \leq F_2^{(k)} \\ x^{(k.j)} - d \leq x \leq x^{(k.j)} + d}} F_1\left(R_s^{(k.j)}(x) \right) \tag{3}$$
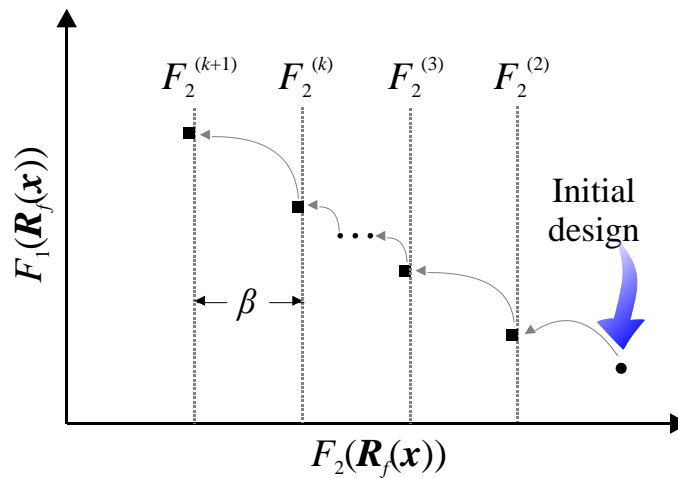

Fig. 1. Conceptual illustration of point-by-point exploration of the Pareto front using the algorithm (1)-(2) [55]. The initial design (black circle) is determined using (1). Subsequently, consecutive Pareto optimal designs (black squares) are obtained sequentially using (2). Vertical dotted lines represent thresholds along objective F_2 (here, $F_2^{(k)} = F_2^{(k-1)} - \beta$).

The surrogate model at iteration j, $R_s^{(k.j)}$, is defined as

$$R_s^{(k.j)}(x) = R_q^{(k.j)}(x) + \left[R_f(x^{(k.j)}) - R_q^{(k.j)}(x^{(k.j)}) \right] \qquad (4)$$

whereas $R_q^{(k.j)}$ is a local approximation model of the low-fidelity model R_c. It is constructed in the interval $[x^{(k.j)} - d, x^{(k.j)} + d]$ which is a vicinity of the current design $x^{(k.j)}$. Solving of (3) is constrained to this interval and the size vector d is determined by the sensitivity analysis of the structure of interest [56]. The approximation model itself is a second-order polynomial model without mixed terms [56], established using $2n + 1$ low-fidelity model evaluations (n is the number of design parameters) allocated using factorial design of experiments (here, a star distribution [26], [36]). More specifically, we have

$$R_q^{(k.j)}(x) = R_q^{(k.j)}([x_1 \ ... \ x_n]^T) = \lambda_0 + \sum_{l=1}^{n} \lambda_l (x_l - x_l^{(k.j)}) + \sum_{l=1}^{n} \lambda_{n+l}(x_l - x_l^{(k.j)})^2 \qquad (5)$$

The model coefficients λ_l are found by solving linear regression problems $R_q^{(k.j)}(x^{(b.l)}) = R_c(x^{(b.l)})$ for $l = 1, \ldots, 2n + 1$, where $x^{(b.l)}$ are the training points.

The size vector d is reduced after each iteration of (3) as $d \leftarrow d/m$ (we use $m = 2$ in our numerical experiments in Section 3). Because of the fact that subsequent Pareto-optimal points are allocated close to each other, only a few iterations of (3) are normally necessary to yield a reasonable approximation of $x^{(k)}$. The correction term in (4) aligns the surrogate and the high-fidelity model at $x^{(k.j)}$, i.e., $R_q^{(k.j)}(x^{(k.j)}) = R_f(x^{(k.j)})$ [50], [57].

2.4. Pareto Front Exploration Using Space Mapping Surrogates

Another option for solving (2) is direct optimization of the surrogate model obtained through appropriate correction of the low-fidelity model using, e.g., space mapping. This approach is practical if the low-fidelity model is cheap. In microwave engineering it would apply to equivalent circuit models, where the structure at hand is described using circuit theory [53]. Equivalent circuit simulation is normally very fast (typically, miliseconds) so that direct optimization of such a model is computationally feasible. There is a large class of structures with reasonably accurate equivalent circuit models, including filters, couplers, power dividers, etc. [58].

Here, we use implicit and frequency space mapping as a low-fidelity model correction technique [56]. The surrogate is defined as

$$\boldsymbol{R}_s(\boldsymbol{x}) = \boldsymbol{R}_{c.F}(\boldsymbol{x}; \boldsymbol{f}, \boldsymbol{p}) \qquad (6)$$

where $\boldsymbol{R}_{c.F}$ is a frequency-scaled low-fidelity model. The vectors $\boldsymbol{f}$ and $\boldsymbol{p}$ denote parameters of the frequency and implicit SM, respectively. The rationale behind frequency scaling is the fact that in microwave/antenna engineering, the model responses are often frequency characteristics so that we have $\boldsymbol{R}_c(\boldsymbol{x}) = [R_c(\boldsymbol{x}, \omega_1) \ R_c(\boldsymbol{x}, \omega_2) \dots R_c(\boldsymbol{x}, \omega_m)]^T$, where $R_c(\boldsymbol{x}, \omega_j)$ is evaluation of the model at a frequency ω_j. Then, $\boldsymbol{R}_{c.F}(\boldsymbol{x}; \boldsymbol{f}, \boldsymbol{p})$ $= [R_c(\boldsymbol{x}, f_0 + \omega_1 \cdot f_1, \boldsymbol{p}) \ \dots \ R_c(\boldsymbol{x}, f_0 + \omega_m \cdot f_1, \boldsymbol{p})]^T$, with f_0 and f_1 being frequency scaling parameters. In other words, frequency scaling allows us to distort the model response along the frequency axis and thus reduce the misalignment between the low- and high-fidelity model [26].

Implicit space mapping [59] is a special type of SM where certain number of parameters (here, denoted using a symbol $\boldsymbol{p}$) are used as additional degrees of freedom for model alignment. These parameters (such as dielectric permittivity and substrate thickness of the microstrip components [35]) are normally fixed in the high-fidelity model but can be freely adjusted in $\boldsymbol{R}_c$.

The SM parameters are extracted to minimize misalignment between $\boldsymbol{R}_s$ and $\boldsymbol{R}_f$ as follows:

$$[\boldsymbol{f}^*, \boldsymbol{p}^*] = \arg \min_{\boldsymbol{f}, \boldsymbol{p}} \| \boldsymbol{R}_f(\boldsymbol{x}) - \boldsymbol{R}_{c.F}(\boldsymbol{x}; \boldsymbol{f}, \boldsymbol{p}) \| \qquad (7)$$

Thus, according to the approach discussed here, the problem (2) is solved using the SM surrogate model and it is itself realized as an iterative process similar to (3)

$$\boldsymbol{x}^{(j.k+1)} = \arg \min_{\boldsymbol{x}, \ F_2(\boldsymbol{R}_s^{(j.k)}(\boldsymbol{x})) \le F_2^{(j)}} F_1\left(\boldsymbol{R}_s^{(j.k)}(\boldsymbol{x})\right) \qquad (8)$$

where

$$\boldsymbol{R}_s^{(j.k)}(\boldsymbol{x}) = \boldsymbol{R}_{c.F}(\boldsymbol{x}; \boldsymbol{f}^{(j.k)}, \boldsymbol{p}^{(j.k)}) \qquad (9)$$

and

$$[\boldsymbol{f}^{(j.k)}, \boldsymbol{p}^{(j.k)}] = \arg \min_{\boldsymbol{f}, \boldsymbol{p}} \| \boldsymbol{R}_f(\boldsymbol{x}^{(j.k)}) - \boldsymbol{R}_{c.F}(\boldsymbol{x}^{(j.k)}; \boldsymbol{f}, \boldsymbol{p}) \| \qquad (10)$$

Similarly as for the technique of Section 2.3, only a few iterations of (8) are normally required to converge.

2.5. Pareto Front Exploration Using Adjoint Sensitivities

In some situations, it is possible to realize fast evaluation of the model derivatives using adjoint sensitivity techniques [9]. Currently adjoints are only supported by a few commercial EM solvers [24], [25]. If cheap derivatives are available, the sub-problem (2) can be efficiently solved using gradient search and trust regions [60] as follows. Similarly as before, $x^{(k)}$ is obtained by local optimization starting from the preceding design $x^{(k-1)}$. The solution to (2) is found iteratively as a sequence $x^{(k.j)}$, $j = 0, 1, \ldots$, with $x^{(k.0)} = x^{(k-1)}$, as

$$x^{(k.j+1)} = \arg \min_{\substack{x,\, F_2(G^{(k.j)}(x)) \leq F_2^{(k)} \\ \|x - x^{(k.j)}\| \leq \delta^{(k.j)}}} F_1\left(G^{(k.j)}(x)\right) \tag{11}$$

where $G^{(k.j)}$ is a linear expansion model of the high-fidelity EM model R_f at $x^{(k.j)}$ defined as

$$G^{(k.j)}(x) = R_f(x^{(k.j)}) + J_{R_f}(x^{(k.j)}) \cdot (x - x^{(k.j)}) \tag{12}$$

Here, $J_{R_f}(x^{(k.j)})$ is a Jacobian of R_f at $x^{(k.j)}$ evaluated using adjoint sensitivities; $\delta^{(k.j)}$ is the trust region radius updated using conventional rules [60]. When using adjoint, computational cost of each iteration of (11), (12) is essentially equal to a single evaluation of the high-fidelity model.

2.6. Pareto Front Exploration Using Response Features

For many classes of microwave and antenna circuits it is possible to reduce the cost of the design process by exploiting so-called feature-based optimization (FBO) approach [41]. FBO takes advantage of the fact that reformulating the design problem in terms of suitably defined response features (e.g., local maxima of the reflection response or frequency location of the −10 dB reflection level [8]) leads to less nonlinear functional landscapes and, therefore, to reduction of the computational cost of the optimization process [61]. Figure 2 shows the family of responses of a microwave filter [41] evaluated along a selected line segment in the design space. It can be observed that the responses are highly nonlinear and change considerably when moving from one design to another. On the other hand, from the point of view of, e.g., minimax optimization as illustrated in Fig. 2(b), only specific characteristic points of the filter responses are important to verify

whether the design satisfies or violates given performance specifications. It turns out that the dependence of these points (both frequency and level coordinates) on geometry parameters of the structure at hand is much less nonlinear as illustrated in Fig. 2(c).

Thus, in FBO, the original problem (here, (2)) is reformulated in terms of the response features so that we have

$$x^{(k)} = \arg \min_{x, \, F_{1.F}(R_{F.f}(x)) \leq F_{1.F}^{(k)}} F_{2.F}\left(R_{F.f}(x)\right) \tag{13}$$

Here, $R_{F.f}(x)$ denotes the vector of the response features extracted from $R_f(x)$, whereas $F_{k.F}$ denote design objectives re-defined in terms of the feature points [61]. FBO produces a sequence $x^{(j.k)}$ of approximations to $x^{(j)}$

$$x^{(j.k+1)} = \arg \min_{\substack{x, \, F_{1.F}(R_{F.f}(x)) \leq F_{1.F}^{(k)} \\ \|x - x^{(j.k)}\| \leq \delta^{(k)}}} F_{2.F}\left(R_l^{(k)}(x)\right) \tag{14}$$

where $R_l^{(k)}$ is a linear approximation model of $R_{F.f}(x)$ at $x^{(j.k)}$ obtained using finite differentiation [60]. As convergence safeguard, $R_l^{(k)}$ is optimized within the trust region of the radius $\delta^{(k)}$. The new design $x^{(j.k+1)}$ is only accepted if $R_{F.f}(x^{(j.k+1)}) < R_{F.f}(x^{(j.k)})$. The trust region radius is updated using the standard rules [60]. To achieve additional speedup, the gradient of $R_{F.f}$ is estimated using the low-fidelity model so that we have
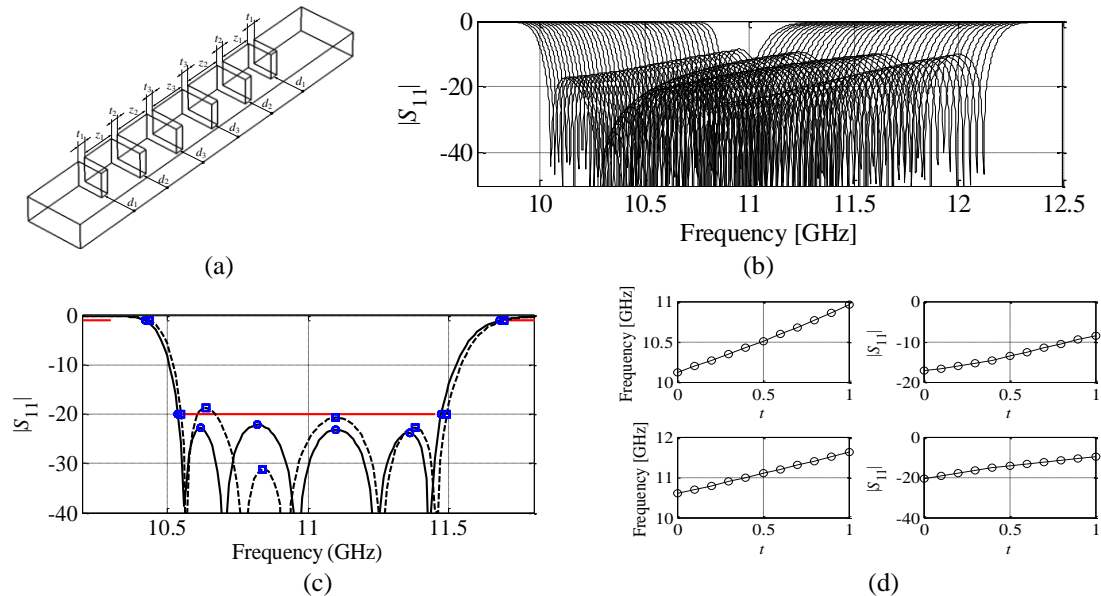

Fig. 2. FBO concept: (a) microwave waveguide filter [41], (b) the family of filter responses evaluated along the line segment parameterized by $0 \leq t \leq 1$, (c) minimax design specifications (response should be above the left and right horizontal lines and below the middle one), (d) variability of selected response features as function of parameter t (cf. Fig. 2(b)).

$$R_l^{(k)}(x) = R_f(x^{(k)}) + \begin{bmatrix} [R_c(x^{(k)} + h_1) - R_c(x^{(k)})]^T / d_1 \\ ... \\ [R_c(x^{(k)} + h_n) - R_c(x^{(k)})]^T / d_n \end{bmatrix}^T \cdot (x - x^{(k)}) \qquad (15)$$

where $h_k = [0 \ldots d_k \ldots 0]^T$ (d_k on kth position). This is justified because even if the low- and high-fidelity models are misaligned in absolute terms, they are normally well correlated so that gradient estimation obtained at the level of the low-fidelity model is a reliable representation of the high-fidelity one [62].

3. Design Case Studies

In this section we demonstrate the algorithm of Section 2 and its variations discussed in Section 2.3-2.6 using several examples of microwave and antenna structures. We also provide comparisons with alternative approaches. The overall discussion and qualitative comparison of algorithm variations are provided in Section 4.

3.1. Case I: Ultrawideband Monopole Antenna

In this section, we illustrate multi-objective optimization using the algorithm of Section 2 and local approximation models as described in Section 2.3. Consider a compact UWB monopole antenna implemented on a 0.762 mm thick Taconic RF-35 substrate ($\varepsilon_r = 3.5$, $h = 0.762$ mm). The structure is shown in Fig. 3. The set of adjustable parameters is $x = [l_g \ g \ a_1 \ a_2 \ l_1 \ l_2 \ w_1 \ s_1 \ s_2 \ o_1 \ o_3]^T$, whereas $w_0 = 1.7$ and $o_2 = 0.5 \cdot a_2$. All dimensions are in mm.

The high-fidelity antenna model R_f contains ~8,000,000 mesh cells and its average simulation time (dual Intel Xeon E5540 machine) is 55 minutes. The low-fidelity model R_c consists of ~100,000 cells and its simulation time is one minute. For the sake of reliability, the SMA connector is included in the simulations. Both models are implemented in CST Microwave Studio and simulated using its transient solver [25].

Two objectives are assumed: F_1 – minimization of the reflection in 3.1 GHz to 10.6 GHz band and F_2 – footprint reduction $S(x)$ defined as $A \times B$ rectangle, where $A = 0.5a_2 + o_1 + o_3$ and $B = l_g + l_1 + w_1$.

The initial design, featuring minimum in-band reflection was obtained from (1). Next, the Pareto-optimal designs were found using (2)-(4). The process was terminated

after the ninth iteration, at which the design with the response being close to the acceptable threshold (i.e., $|S_{11}| \leq -10$ dB in the UWB band) was found.

The obtained Pareto-optimal designs are shown in Fig. 4. Their dimensions and frequency characteristics (for the selected antenna realizations) are provided in Table 1 and Fig. 5, respectively. The span of the Pareto front along F_1 and F_2 is 6 dB (from -16 dB to -10 dB) and 120 mm^2 (from 300 mm^2 to 180 mm^2), respectively.

Numerical cost of multi-objective optimization corresponds to only 48 evaluations of the high-fidelity antenna model. It includes: 350 and 4 evaluations of the low- and high-fidelity model evaluations for obtaining the starting point, as well as 46 $\boldsymbol{R}_c$ and 3 $\boldsymbol{R}_f$ simulations per iteration to find consecutive Pareto-optimal designs.
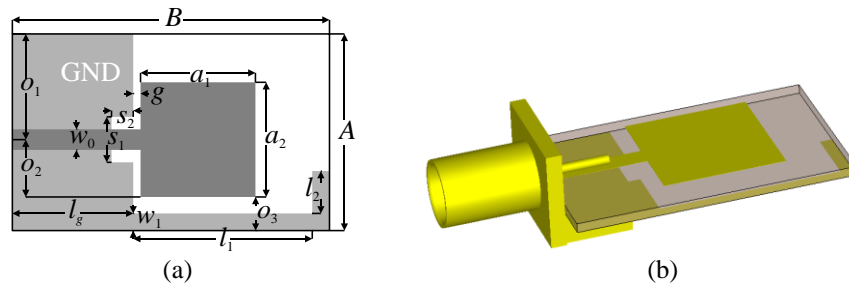

Fig. 3. Compact UWB monopole antenna [55]: (a) geometry; (b) 3D EM model with connector.
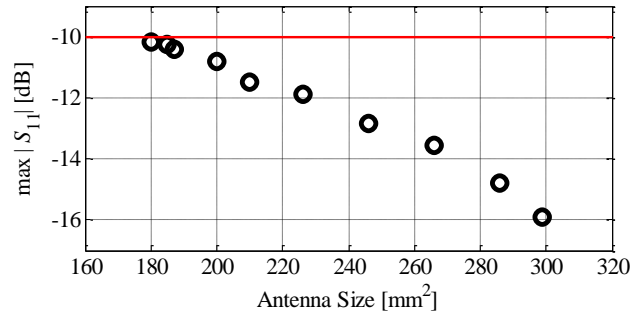

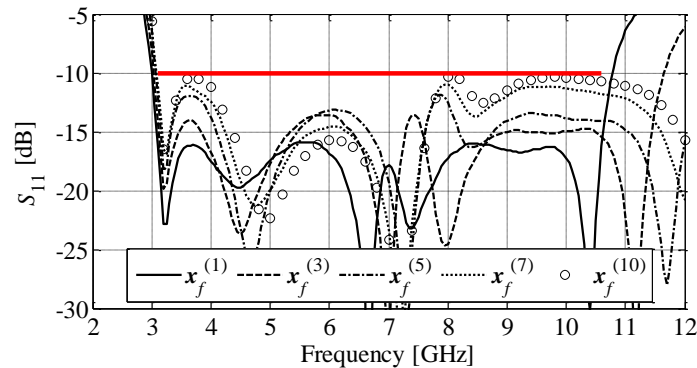Fig. 4. Pareto-optimal set of the compact UWB monopole obtained using method of Section 2.3 [55].

Fig. 5. Frequency responses of the selected UWB monopole antenna designs (for corresponding antenna dimensions, see Table 1) [55].

Table 1: Compact UWB Monopole Antenna: Dimensions of Pareto-Optimal Designs

$x_f^{(k)}$	Design Variables [mm]											max $\|S_{11}\|$ [dB]	Area [mm^2]
	l_g	g	a_1	a_2	l_1	l_2	w_1	s_1	s_2	o_1	o_3		
1	6.79	0.44	9.84	9.07	13.5	5.71	1.49	3.06	1.69	6.44	2.74	−15.9	299
2	6.51	0.56	9.43	8.93	13.3	5.71	1.45	3.21	1.46	6.48	2.49	−14.8	286
3	6.46	0.63	9.25	8.47	13.1	5.87	1.31	3.25	1.55	6.35	2.18	−13.6	266
4	6.28	0.69	8.99	7.91	12.9	5.92	1.19	2.29	1.68	6.25	1.89	−12.8	246
5	5.98	0.73	8.79	7.47	12.6	6.07	1.13	3.31	1.81	6.11	1.60	−11.9	226
6	5.30	0.87	8.77	6.93	12.4	6.25	1.50	3.43	2.00	6.18	1.28	−11.5	210
7	5.39	0.82	8.51	6.62	12.2	6.36	1.32	3.25	2.00	5.94	1.31	−10.7	200
8	5.16	0.81	8.52	6.34	12.0	6.57	1.48	3.37	2.00	5.93	0.92	−10.4	190
9	5.18	0.83	8.49	6.31	12.0	6.56	1.45	3.37	2.00	5.90	0.89	−10.3	185
10	4.98	0.85	8.56	6.27	12.1	6.64	1.48	3.49	2.00	5.85	0.73	−10.2	180

The presented optimization approach was compared with two multi-objective evolutionary algorithm-based (MOEA) methods [12], [51]. The first method directly utilizes R_c antenna model for MOEA optimization (algorithm setup: population size 100, number of iterations 100), whereas the second executes MOEA on kriging model constructed from R_c model data (MOEA setup: 500 individuals, 50 iterations) [28], [50].

The reason for performing comparison based on the low-fidelity model simulations is that the cost of direct MOEA optimization using high-fidelity model (10000 R_f model evaluations corresponds to 382 days of CPU-time) is prohibitive. For fair comparison, benchmark methods were executed in a search space region defined by the designs $x_f^{(1)}$ and $x_f^{(10)}$ (cf. Table 1). The obtained results are compared in Fig. 6. It should be noted that the obtained Pareto front representations noticeably vary along F_2 (differences along F_1 are below 1.5 dB). Narrower MOEA-based Pareto sets can be explained by limited exploration capability of the algorithm in the vicinity of the 11-dimensional design space corners. Also, limited number of R_c evaluations led the first benchmark method to capture only half of the Pareto front. The optimization cost (excluding CPU-time required for obtaining the extreme Pareto designs) is 10000 R_c (~167 hours) and 802 R_c simulations (~13.4 hours) for the first and second benchmark approach, respectively, whereas only 460 R_c evaluations (~7.7 hours of CPU-time) were required to find the Pareto set using our method.

The results indicate that, for the considered problem, the point-by-point algorithm reduces the cost of multi-objective optimization compared to MOEA-based techniques (from almost 43 percent to over 93 percent), while ensuring similar (or better) quality of Pareto front.

3.2. Case II: Miniaturized Rat-Race Coupler

Our second design problem is a miniaturized rat-race coupler (RRC) of Fig. 7(a). For such structures, there are reasonably good equivalent circuit models available which allows us to use space mapping surrogate models as described in Section 2.4. Design parameters are $x = [l_1 \ l_2 \ l_3 \ d \ w]^T$, with $w_0 = 1.7$, $l_0 = 15$ fixed (all dimensions in mm). The low- and high-fidelity models of the structure are implemented in Agilent ADS [MWCL7] and CST Microwave Studio [MWCL8] (~220,000 mesh cells, CPU-time: ~15 min), respectively. The EM model is implemented on the Taconic RF-35 (see Section 3.1). The surrogate model is constructed using frequency SM as well as implicit SM with preassigned parameters p being dielectric permittivity and substrate thickness of the microstrip components of the circuit corresponding to $p = [\varepsilon_1 \ \varepsilon_2 \ \varepsilon_3 \ h_1 \ h_2 \ h_3]^T$ (see also Fig. 7(b)).

The design objectives are: F_1 – maximization of bandwidth (given as intersection of frequency ranges for which both $|S_{11}| \le -20$ dB and $|S_{41}| \le -20$ dB) and F_2 – size reduction. Moreover, a suitably defined penalty function ensures 3 dB split at the center frequency.

Similarly as in Section 3.1, solution to (1) has been found to identify the starting point for the algorithm of Section 2.4. The remaining designs have been obtained sequentially by optimizing the space mapping surrogate model. The obtained Pareto set is shown in Fig. 8(a). The variability of the Pareto front along F_1 and F_2 is 245 mm^2 and 206 MHz, respectively.
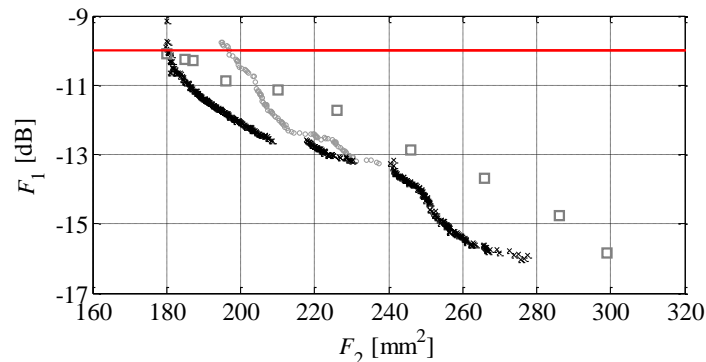

Fig. 6. Comparison of low-fidelity Pareto-optimal sets obtained using point-by-point algorithm (□), as well as MOEA optimization of R_c (○) and kriging interpolation (×) models [55].

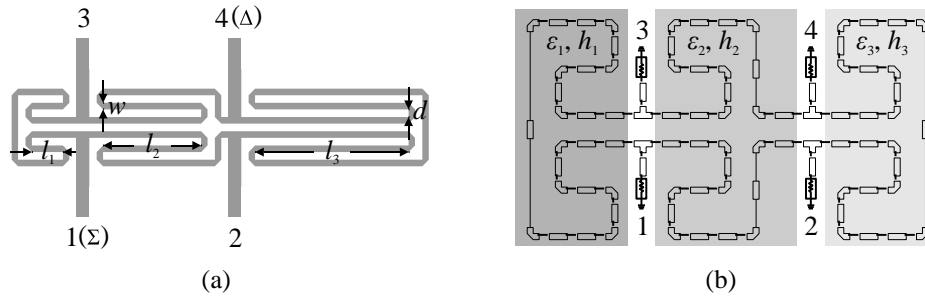(a)   (b)

Fig. 7. Folded RRC [53]: (a) layout (CST Studio); (b) equivalent circuit model (Agilent ADS). Highlighted regions correspond to different sets of implicit SM parameters $\boldsymbol{p}$.

(a)   (b)

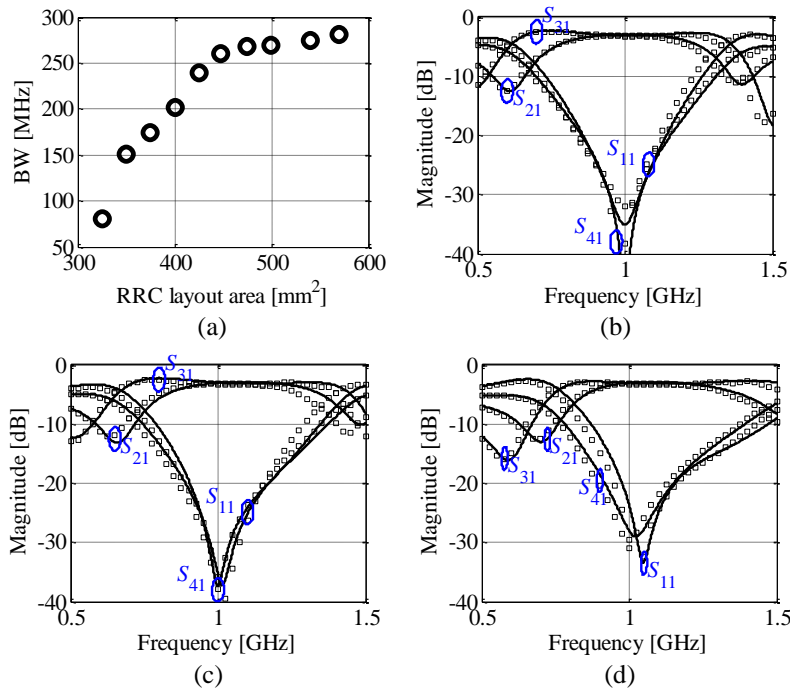
(c)   (d)

Fig. 8. Point-by-point optimization of the space mapping-based compact coupler surrogate [53]: (a) Pareto set; (b)-(d) Simulated (—) and measured (□) characteristics of selected designs: (b) $\boldsymbol{x}_f^{(1)}$; (c) $\boldsymbol{x}_f^{(5)}$; (d) $\boldsymbol{x}_f^{(8)}$.

Table 2. Multi-Objective RRC Optimization: Dimensions of Selected Pareto-Optimal Designs

	Design Variables [mm]					Objectives		Miniaturization[*] [%]
	l_1	l_2	l_3	d	W	BW [MHz]	Layout Area [mm^2]	
$\boldsymbol{x}_f^{(1)}$	4.18	13.20	20.68	0.994	0.865	281	570	90.8
$\boldsymbol{x}_f^{(3)}$	3.83	11.76	20.44	0.825	0.877	270	500	91.9
$\boldsymbol{x}_f^{(5)}$	4.10	13.78	21.14	0.581	0.887	260	450	92.7
$\boldsymbol{x}_f^{(7)}$	4.25	12.17	22.12	0.400	0.923	202	400	93.5
$\boldsymbol{x}_f^{(8)}$	3.95	10.87	21.71	0.350	0.936	174	375	93.9
$\boldsymbol{x}_f^{(9)}$	4.37	12.33	22.52	0.350	0.820	151	350	94.3

[*] With respect to conventional RRC (radius = 44.39 mm, size = 6190 mm^2).

The design cost corresponds about 30 high-fidelity model simulations (~7.5 hours of CPU-time), including the overhead for the circuit model $\boldsymbol{R}_c$ evaluations. The latter is below 20 percent with respect to overall design cost. It should be noted that the estimated cost of direct MOEA-based optimization of the coupler (setup: 100 individuals; 100 iterations) is 10,000 high-fidelity model evaluations (100 days of CPU-time).

3.3. Case III: Miniaturized Impedance Matching Transformer

In order to illustrate utilization of adjoint sensitivities for solving the sub-problem (2) consider a miniaturized 50 ohm to 130 ohm impedance matching transformer implemented on the Taconic RF-35 (see Fig. 9) [63]. The vector of adjustable parameters is $\boldsymbol{x} = [w_{11}\ w_{21}\ w_{31}\ l_{21}\ l_{31}\ w_{12}\ w_{22}\ w_{32}\ l_{22}\ l_{32}\ w_{13}\ w_{23}\ w_{33}\ l_{23}\ l_{33}]^T$. Dimensions $w_{i1} = 1.7$ and $w_{i2} = 0.15$ remain fixed to ensure the required source and load impedances (all in mm).

The transformer has been optimized using the method of Section 2.5. The response characteristics and their gradients are obtained from the computational model $\boldsymbol{R}_f$ implemented in Ansys HFSS (~8000 tetrahedrons, average simulation time on a dual Intel Xeon E5540 machine is 34 min) and exploiting adjoint sensitivities [24]. Design objectives are as follows: F_1 – minimization of reflection defined as $\max(|S_{11}|_{3.1\text{ GHz to }10.6\text{ GHz}})$ and F_2 – transformer miniaturization ($F_2(\boldsymbol{x}) = A \times B$ rectangle, where $A = 2\cdot(l_{21} + l_{31}) + w_{21} + w_{12} + 2\cdot(l_{22} + l_{32}) + w_{22} + w_{13} + 2\cdot(l_{23} + l_{33}) + w_{23}$ and $B = w_{11} + w_{31} + l_{31}$).

The initial design has been found by unconstrained optimization with respect to F_1. Subsequently, the Pareto set has been found by solving (2) using adjoint sensitivities (Section 2.5). The obtained high-fidelity Pareto set is shown in Fig. 10, whereas the dimensions of the selected designs are provided in Table 3. The smallest design features footprint of 6 mm^2 and the in-band reflection close to -10 dB (acceptable threshold value). Frequency responses of the transformer at designs of Table 3 are shown in Fig. 11.

The cost of multi-objective optimization is 60 evaluations of the EM simulation model $\boldsymbol{R}$ (~34 hours of CPU-time) including 10 evaluations required to find the initial design and three to four evaluations to find the subsequent designs (the cost per design).
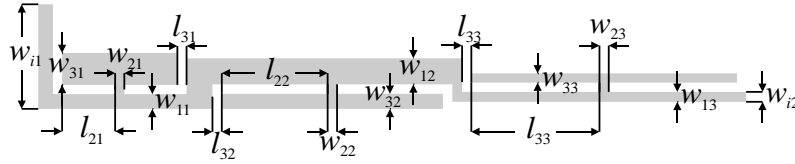
Fig. 9. Geometry of a compact, three section 50 Ohm to 130 Ohm matching transformer [63].

Table 3: Matching Transformer Optimization Results

| Selected designs		$x_f^{(1)}$	$x_f^{(5)}$	$x_f^{(9)}$	$x_f^{(13)}$	$x_f^{(16)}$
$F_1 - |S_{11}|$ [dB]		−9.9	−12.8	−14.9	−15.9	−16.4
F_2 – area [mm²]		6.0	9.9	14.0	18.0	21.2
Design variables	w_{11}	0.247	0.539	0.583	0 .622	0.593
	w_{21}	0.693	0.696	0.699	0.493	0.319
	w_{31}	0.150	0.150	0.202	0.418	0.595
	l_{21}	2.417	2.275	2.554	2.111	1.757
	l_{31}	0.150	0.150	0.153	0.151	0.242
	w_{12}	0.150	0.151	0.151	0.371	0.461
	w_{22}	0.150	0.150	0.151	0.292	0.300
	w_{32}	0.240	0.375	0.385	0.225	0.152
	l_{22}	1.000	1.357	1.904	2.085	2.159
	l_{32}	0.155	0.238	0.182	0.177	0.256
	w_{13}	0.150	0.150	0.154	0.153	0.150
	w_{23}	0.150	0.157	0.215	0.306	0.319
	w_{33}	0.177	0.276	0.150	0.151	0.183
	l_{23}	1.000	1.083	1.832	2.059	2.092
	l_{33}	0.150	0.168	0.150	0.150	0.155
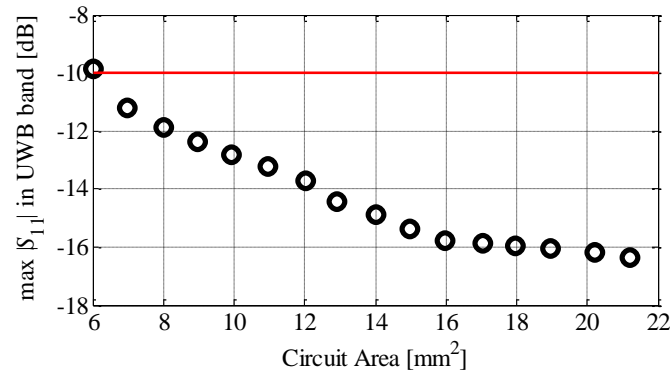
Fig. 10. Representation of Pareto front obtained by means of the multi-objective algorithm of Section 2.5.
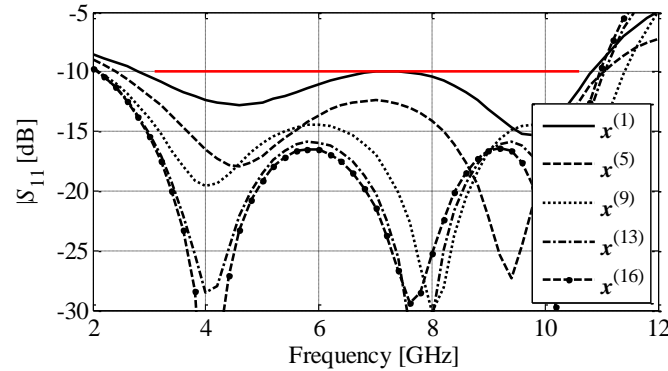
Fig. 11. Transformer responses at the selected Pareto-optimal designs. Design symbols correspond to the data gathered in Table 3.

3.4. Case IV: UWB Monopole Antenna

Our last illustration example is again the UWB monopole considered in Section 3.1. As a matter of fact, it is a simplified version of the structure of Fig. 3 [4] which does not feature a slit below the feeding line. The antenna geometry is shown in Fig. 12. The substrate is the same as for the remaining structures. The design variables are $x = [w_0 \ g \ a_1 \ a_2 \ l_1 \ l_2 \ w_1 \ o]^T$. Parameter $w_0 = 2o + a_2$, whereas $w_i = 1.7$ is fixed (all dimensions in mm).

The EM models are implemented in CST Studio (R_f: ~4,600,000 mesh cells, simulation: 40 min, and R_c : ~850,000 cells, 2 minutes). The models include the SMA connector (see Fig. 12(b)). The design objectives are the same as in Section 3.1.

In this case, the problem (2) is solved using the feature-based optimization approach (cf. Section 2.6). The feature points utilized in the optimization process include the local maxima of the reflection response as well as the point corresponding to the required reflection level (the antenna is optimized to) in the vicinity of the lower edge of the operational bandwidth (cf. Fig. 13).
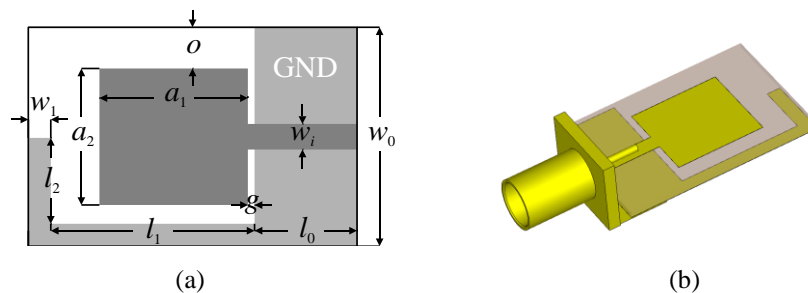

(a)	(b)

Fig. 12. UWB monopole antenna [54]: (a) top view with highlighted design parameters, (b) 3D view.

The initial Pareto-optimal design has been obtained as in (1) using a combination of pattern search [64] and feature-based optimization [54]. The maximum in-band reflection at this design is −13.5 dB. The remaining Pareto optimal designs have been obtained by applying the feature-based approach (cf. Section 2.6) for solving (2). The variability of the Pareto front along objectives F_1 and F_2 is 46 mm^2 and −3.5 dB, respectively. Detailed dimensions of selected Pareto designs are gathered in Table 4.
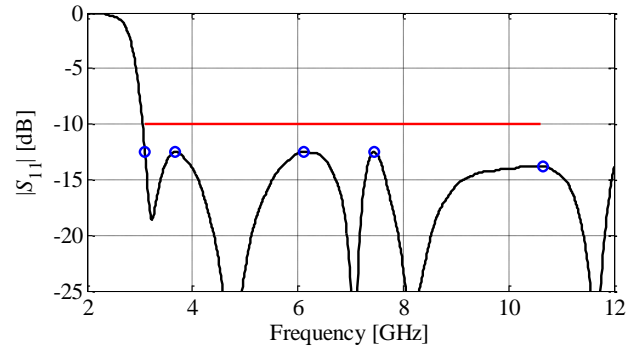

Fig. 13. UWB monopole antenna: feature points (o) utilized in the multi-objective optimization process [54].
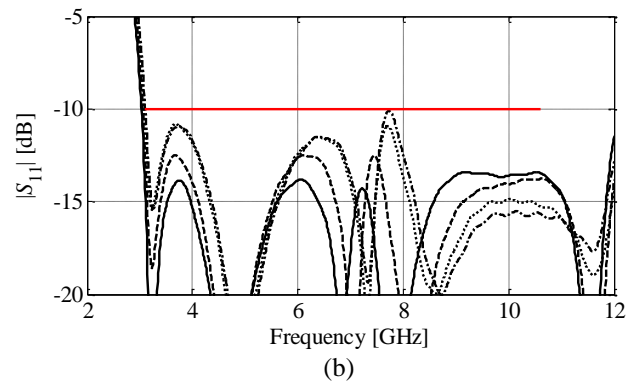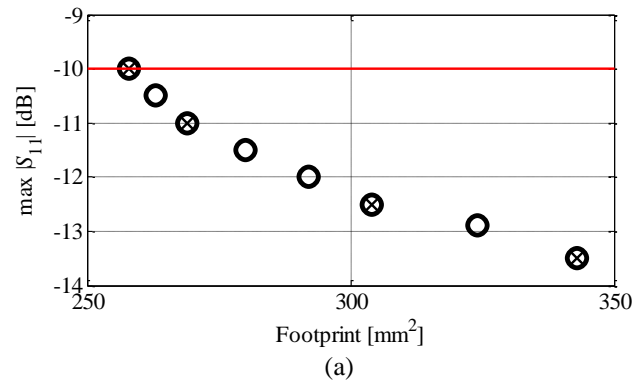

(a)

(b)

Fig. 14. Optimization results of the UWB monopole antenna of Fig. 12 [54]: (a) Pareto set for obtained using the feature-based method; and (b) frequency characteristics of the antenna at the selected Pareto-optimal designs $x^{(1)}$ (——), $x^{(3)}$ (- - -), $x^{(6)}$ (····), and $x^{(8)}$ (·-··-·).

Table 4. Selected Pareto-optimal Antenna Designs

Design	Size [mm^2]	max $|S_{11}|$ [dB]	Antenna dimensions in mm							
			w_0	g	a_1	a_2	l_1	l_2	w_1	o
$x^{(1)}$	343	−13.5	6.00	0.77	8.93	10.29	12.75	5.20	2.45	2.94
$x^{(3)}$	304	−12.5	5.69	0.80	8.99	9.96	12.63	5.78	1.89	2.52
$x^{(6)}$	269	−11.0	5.13	0.80	9.14	9.04	12.40	6.35	1.75	2.46
$x^{(8)}$	258	−10.0	5.06	0.78	9.12	8.94	12.36	6.38	1.64	2.30

Figure 14 shows the Pareto set representation obtained using the proposed approach as well as the antenna reflection responses at the selected Pareto-optimal designs from Table 4. The total optimization cost corresponds to only about 28 evaluations of R_f (~25 hours of CPU-time) including 208 simulations of the low-fidelity model R_c and 17 evaluations of the high-fidelity model R_f. For the sake of comparison, the cost of antenna optimization using local approximation models (Section 2.3) was higher (45 equivalent evaluations of R_f including 411 evaluations of the low- fidelity model and 24 evaluations of the high-fidelity one). Furthermore, the cost of the expedited MOEA-based optimization [65] is about 67 evaluations of the high-fidelity model (including ~200 R_c model evaluations for extreme Pareto designs identification, ~650 R_c model simulations for construction of the the kriging model of the antenna and three R_f model simulations for output space mapping-refinement (per sample)).

4. Discussion and Conclusion

In this paper, a deterministic approach for rapid multi-objective optimization of expensive computational electromagnetics models has been discussed. The methodology exploits point-by-point exploration of the Pareto front using local search. We reviewed a basic version of the procedure and proposed a few alternative variations exploiting space mapping surrogates, adjoint sensitivities as well as response features. The technique allows for rapid identification of the set of Pareto-optimal designs. The computational complexity of the procedure is competitive to the methods using population-based metaheuristics (either directly or with auxiliary response surface approximation models). There were four variations of the methods discussed. The basic one using local approximation models is a generic approach suitable for a wide class of problems in microwave and antenna engineering. The other three variations are more specific. In

particular, availability of fast low-fidelity models (such as equivalent circuits) permits utilization of space mapping surrogates as described in Section 2.4. Availability of cheap adjoint sensitivities permits rapid solution of the local optimization sub-problems using gradient search with trust regions (Section 2.5). Finally, in some cases it is possible to further speed up the optimization process by exploiting response features (cf. Section 2.6 and 3.4) where the original problem is reformulated in terms of the feature points which simplified the functional landscape to be optimized. In terms of selecting a particular variation of the presented optimization technique, including additional tools and models (if available) is recommended as it normally leads to reducing the cost of the design process. Most of the presented variations utilize variable-fidelity simulation models. The typical cost of generating a Pareto set is a few dozen of high-fidelity simulations, which is very low compared to techniques based on metaheuristics. Finally, it should be mentioned that although the presented technique is not generic (e.g., it might not work well if the Pareto front is not a connected set in the design space) it is well suited for problems in computational electromagnetics as illustrated using a variety of microwave and antenna structures. Generalization of the algorithm for a larger number of objectives will be considered in a future work.

Acknowledgement

References

[1]   P. Kurgan, A. Bekasiewicz, M. Pietras, and M. Kitlinski, "Novel topology of compact coplanar waveguide resonant cell low-pass filter," *Microwave Opt. Techn. Lett.*, vol. 54, no. 3, pp. 732-735, 2012.

[2]   M. Bod, H.R. Hassani, and M.M.S Taheri, "Compact UWB printed slot antenna with extra Bluetooth, GSM, and GPS bands," *IEEE Ant. Wireless Prop. Lett.*, vol. 11, pp. 531-534, 2012.

[3]   S. Koziel and S. Ogurtsov, "Fast simulation-driven design of integrated photonic components using surrogate models," to appear, *IET Microwaves, Antennas Prop.*, 2014.

[4]   A. Costanzo, M. Dionigi, D. Masotti, M. Mongiardo, G. Monti, L. Tarricone, and R. Sorrentino, „Electromagnetic energy harvesting and wireless power transmission: a unified approach," *Proc. IEEE*, vol. 102, no. 11, pp. 1692-1711, 2014.

[5]   K. Moussakhani, R.K. Amineh, and N.K. Nikolova, „Estimating the efficiency of antennas used as sensors in microwave tissue measurements," *IEEE Trans. Ant. Prop.*, vol. 62, no. 1, pp. 295-301, 2014.

[6]   Y. Gotoh, A. Kiya, and N. Takahashi, „Electromagnetic inspection of outer side defect on steel tube with steel support using 3-D nonlinear FEM considering non-uniform permeability and conductivity," *IEEE Trans. Magn.*, vol. 46, no. 8, pp. 3145-3148, 2010

[7]   J.W. You, S.R. Tan, X.Y. Zhou, W.M. Yu, and T.J. Cui, "A new method to analyze broadband antenna-radome interactions in time-domain," *IEEE Trans. Ant. Prop.*, vol. 62, no. 1, pp. 334-344, 2014.

[8]   A. Bekasiewicz and S. Koziel, "Structure and computationally-efficient simulation-driven design of compact UWB monopole antenna," *IEEE Antennas and Wireless Propagation Letters*, vol. 14, pp. 1282-1285, 2015.

[9]   S. Koziel, and A. Bekasiewicz, "Variable-fidelity optimization of antennas using adjoint sensitivities," *Loughborough Antennas & Propagation Conference*, pp. 412-415, Loughborough, 2014.

[10]   J. Nocedal and S. Wright, *Numerical Optimization*, 2nd edition, Springer, New York, 2006.

[11]   A. Conn, K. Scheinberg, and .N. Vincente, *Introduction to Derivative-Free Optimization*, MPS-SIAM Series on Optimization, Philadelphia, 2009.

[12]   K. Deb, *Multi-Objective Optimization Using Evolutionary Algorithms.* New York, NY, USA: Wiley, 2001.

[13]   N. Jin and Y. Rahmat-Samii, "Advances in particle swarm optimization for antenna designs: real-number, binary, single-objective and multiobjective implementations," *IEEE Tran. Antennas Propag.*, vol. 55, no. 3, pp. 556-567, 2007.

[14]   W. Wang, S. Gong, X. Wang, Y. Guan, and W. Jiang, „Differential evolution algorithm and method of moments for the design of low-RCS antenna," *IEEE Ant. Wireless Prop. Lett.*, vol. 9, pp. 295-298, 2010.

[15]   X. Qing and Z.N. Chen, "Compact coplanar waveguide-fed ultra-wideband monopole-like slot antenna," *IET Microwaves Ant. Prop.*, vol. 3, no. 5, pp. 889-898, 2009.

[16]   Y.-M. Pan, K.W. Leung, and K. Lu, „Compact quasi-isotropic dielectric resonator antenna with small ground plane," *IEEE Trans. Ant. Prop.*, vol. 62, no. 2, pp. 577-585, 2014.

[17]   P.A.W. Basl, M.H. Bakr, and N.K. Nikolova, "Theory of self-adjoint *S*-parameter sensitivities for lossless nonhomogeneous transmission-line modeling problems," *IET Microwaves, Ant. Prop.*, vol. 2, no. 3, pp. 211-220, 2008.

[18]   M.H. Bakr and N.K. Nikolova, "An adjoint variable method for time domain TLM with wideband Johns matrix boundaries," *IEEE Trans. Microwave Theory Tech.*, vol. 52, no. 2, pp. 678-685, 2004.

[19]   S. Koziel and A. Bekasiewicz, "Fast EM-driven size reduction of antenna structures by means of adjoint sensitivities and trust regions," *IEEE Ant. Wireless Prop. Lett.*, vol. 14, pp. 1681-1684, 2015.

[20]   A. Bekasiewicz and S. Koziel, "Efficient multi-fidelity design optimization of microwave filters using adjoint sensitivity," *Int. J. RF and Microwave CAE*, vol. 25, no. 2, pp. 178-183, 2015.

[21]   S.W. Director and R.A. Rohrer, "The generalized adjoint network and network sensitivities," *IEEE Trans. Circuit Theory*, vol. 16, pp. 318–323, 1969.

[22]   J.W. Bandler and R.E. Seviora, "Wave sensitivities of networks," *IEEE Trans. Microwave Theory Tech.*, vol. 20, pp. 138–147, 1972.

[23]   D. Li and P. Hartman, "Adjoint-based airfoil optimization with discretization error control," Int. J. Numerical Methods in Fluids, vol.77, no.1, pp. 1-17, 2015.

[24] Ansys HFSS, ver. 14.0 (2012), ANSYS, Inc., Southpointe 275 Technology Dr., Canonsburg, PA.

[25] CST Microwave Studio, ver. 2014, CST AG, Bad Nauheimer Str. 19, D-64289 Darmstadt, Germany, 2014.

[26] S. Koziel and X.S. Yang (Eds.), "Computational optimization, methods and algorithms," Series: Studies in Computational Intelligence, vol. 356, Springer, 2011.

[27] N.V. Queipo, R.T. Haftka, W. Shyy, T. Goel, R. Vaidynathan, and P.K. Tucker, "Surrogate-based analysis and optimization," *Progress in Aerospace Sciences*, vol. 41, no. 1, pp. 1-28, Jan. 2005.

[28] A.I.J. Forrester and A.J. Keane, "Recent advances in surrogate-based optimization," *Progress in Aerospace Sciences*, vol. 45, pp. 50-79, 2009.

[29] Y. Jin, "Surrogate-assisted evolutionary computation: Recent advances and future challenges," *Swarm and Evolutionary Computation*, vol. 1, no. 2, pp. 61-70, 2011.

[30] F.J. Villegas, T. Cwik, Y. Rahmat-Samii, and M. Manteghi, „A parallel electromagnetic genetic-algorithm optimization (EGO) application for patch antenna design," *IEEE Transactions on Antennas and Propagation*, vol. 52, no. 9, pp. 2424-2435, 2004.

[31] J. Knowles, „ParEGO: a hybrid algorithm with on-line landscape approximation for expensive multiobjective optimization problems," *IEEE Transactions on Evolutionary Computation*, vol. 10, no. 1, pp. 50-66, 2006.

[32] D.R.B. de Araújo, C.J.A. Bastos-Filho, and J.F. Martins-Filho, „An evolutionary approach with surrogate models and network science concepts to design optical networks," Engineering Applications of Artificial Intelligence, vol. 43, pp. 67-80, 2015.

[33] Y.-S. Ong, P.B. Nair, and K.Y. Lum, „Max-min surrogate-assisted evolutionary algorithm for robust design," *IEEE Trans. Evolutionary Computation*, vol. 10, no. 4, pp. 392-404, 2006.

[34] B. Liu, Q. Zhang, and G.G.E. Gielen, „A Gaussian Process Surrogate Model Assisted Evolutionary Algorithm for Medium Scale Expensive Optimization Problems," *IEEE Transactions on Evolutionary Computation*, vol. 18, no. 2, pp. 180-192, 2014.

[35] A. Bekasiewicz, P. Kurgan, and M. Kitlinski, "A new approach to a fast and accurate design of microwave circuits with complex topologies," *IET Microwaves, Antennas & Propagation*, vol. 6, no. 14, pp. 1616-1622, 2012.

[36] J.W. Bandler, Q.S. Cheng, S.A. Dakroury, A.S. Mohamed, M.H. Bakr, K. Madsen, and J. Søndergaard, "Space mapping: the state of the art," *IEEE Trans. Microwave Theory Tech.*, vol. 52, no. 1, pp. 337-361, Jan. 2004.

[37] S. Koziel and J.W. Bandler, "Space mapping with multiple coarse models for optimization of microwave components," *IEEE Microwave and Wireless Components Letters*, vol. 18, pp. 1-3, 2008.

[38] S. Koziel, J.W. Bandler, and K. Madsen, "Space mapping with adaptive response correction for microwave design optimization," *IEEE Trans. Microwave Theory Tech.*, vol. 57, no. 2, pp. 478-486, 2009.

[39] S. Koziel, S. Ogurtsov, and S. Szczepanski, "Rapid antenna design optimization using shape-preserving response prediction," *Bulletin of the Polish Academy of Sciences. Technical Sciences*, vol. 60, no. 1, pp. 143-149, 2012.

[40] S. Koziel and L. Leifsson, "Multi-point response correction for reduced-cost EM-simulation-driven design of antenna structures," *Microwave Opt. Tech. Lett.*, vol. 55, no. 9, pp. 2070-2074, 2013.

[41] S. Koziel and J.W. Bandler, "Rapid yield estimation and optimization of microwave structures exploiting feature-based statistical analysis," *IEEE Trans. Microwave Theory Tech.*, vol. 63, no., 1, pp. 107-114, 2015.

[42] S. Koziel, "Adaptively adjusted design specifications for efficient optimization of microwave structures," *Progress in Electromagnetic Research B*, vol. 21, pp. 219-234, 2010.

[43] S. Koziel and A. Bekasiewicz, "Rapid simulation-driven design of miniaturized dual-band microwave couplers by means of adaptive response scaling," to appear, *IET Microwaves, Ant. Prop.*, 2016.

[44] B. Mun, C. Jung, M.-J. Park, and B. Lee „A compact frequency-reconfigurable multiband LTE MIMO antenna for laptop applications," *IEEE Ant. Wireless Prop. Lett.*, vol. 13, pp. 1389-1392, 2014.

[45] N. Chahat, M. Zhadobov, R. Sauleau, and K. Ito, "A compact UWB antenna for on-body applications," *IEEE Trans Ant. Prop.*, vol. 59, no. 4, pp. 1123-1131, 2011.

[46] Y. Kuwahara, "Multiobjective optimization design of Yagi–Uda antenna," *IEEE Tran. Antennas Propag.*, vol. 53, no. 6, June 2005, pp. 1984-1992.

[47] S. Chamaani, M.S. Abrishamian, and S.A. Mirtaheri, "Time-domain design of UWB Vivaldi antenna array using multiobjective particle swarm optimization," *IEEE Antennas and Wireless Prop. Lett.*, vol. 9, pp. 666-669, 2010.

[48] S. Kukkonen and J. Lampinen, "An extension of generalized differential evolution for multi-objective optimization with constraints," *Parallel Problem Solving from Nature*, pp. 752–761, 2004.

[49] N.K. Madavan, "Multiobjective optimization using a Pareto differential evolution approach," *Congress Evol. Comp.*, vol. 2, pp. 1145–1150, 2002.

[50] S. Koziel, and S. Ogurtsov, "Multi-objective design of antennas using variable-fidelity simulations and surrogate models," *IEEE Trans. Ant. Prop.*, vol. 61, no. 12, pp. 5931-5939, 2013.

[51] S. Koziel, A. Bekasiewicz, and W. Zieniutycz, "Expedite EM-driven multi-objective antenna design in highly-dimensional parameter spaces," *IEEE Ant. Wireless Prop. Lett.*, vol. 13, pp. 631-634, 2014.

[52] S. Koziel and A. Bekasiewicz, "Fast multi-objective surrogate-assisted design of multi-parameter antenna structures through rotational design space reduction," *IET Microwaves, Ant. Prop.*, vol. 10, no. 6, pp. 624-630, 2016.

[53] S. Koziel, A. Bekasiewicz, and P. Kurgan, "Rapid multi-objective simulation-driven design of compact microwave circuits," *IEEE Microwave Wireless Comp. Lett.*, vol. 25, no. 5, pp. 277-279, 2015.

[54] S. Koziel and A. Bekasiewicz, "Low-cost multi-objective optimization of antennas using Pareto front exploration and response features," to appear, *IEEE Int. Symp. Ant. Prop.*, Fajardo, 2016.

[55] S. Koziel and A. Bekasiewicz, "Rapid multi-objective antenna design using point-by-point Pareto set identification and local surrogate models," *IEEE Trans. Ant. Prop.*, vol. 64, no. 6, pp. 2551-2556, 2016.

[56] S. Koziel and S. Ogurtsov, "Antenna design by simulation-driven optimization," Springer, 2014.

[57] N.M. Alexandrov and R.M. Lewis, "An overview of first-order model management for engineering optimization," *Optimization Eng.*, vol. 2, no. 4, pp. 413-430, Dec. 2001.

[58] D.M. Pozar, "Microwave Engineering," 4th ed., John Wiley & Sons, 2012.

[59] J.W. Bandler, Q.S. Cheng, N.K. Nikolova, and M.A. Ismail, "Implicit space mapping optimization exploiting preassigned parameters," *IEEE Trans. Microwave Theory Tech.*, vol. 52, no. 1, pp. 378-385, 2004.

[60] A. Conn, N.I.M. Gould, and P.L. Toint, *Trust-region methods*, MPS-SIAM Series on Optimization, Philadelphia, 2000.

[61] S. Koziel and S. Ogurtsov, "Fast surrogate-assisted simulation-driven optimisation of add-drop resonators for integrated photonic circuits," *IET Microwaves, Antennas Prop.*, vol. 9, no. 7, pp. 672-675, 2015.

[62] O. Glubokov and S. Koziel, "EM-driven tuning of substrate integrated waveguide filters exploiting feature-space surrogates," *Int. Microwave Symp.*, Tampa Bay, FL, USA, pp. 1-3, 2014.

[63] P. Kurgan, A. Bekasiewicz, and M. Kitlinski, "On the low-cost design of abbreviated multi-section planar matching transformer," *Microwave Opt. Techn. Lett.*, vol. 57, no. 3, pp. 521-525, 2015.

[64] T.G. Kolda, R.M. Lewis, and V. Torczon, "Optimization by direct search: new perspectives on some classical and modern methods," *SIAM Review*, vol. 45, no. 3, pp. 385–482, 2003.

[65] S. Koziel and A. Bekasiewicz, "Recent developments in simulation-driven multi-objective design of antennas," *Bulletin of the Polish Academy of Sciences. Technical Sciences*, vol. 63, no. 3, pp. 781-789, 2015.